Circular orbits and polarized images of charged particles orbiting a Kerr black hole with a weak magnetic field

Tsaichen Lee,[1] Zezhou Hu[1] Minyong Guo[2,*] and Bin Chen[1,3,4]

[1]*Department of Physics, Peking University,*
No. 5 Yiheyuan Road, Beijing 100871, People's Republic of China
[2]*Department of Physics, Beijing Normal University, Beijing 100875, People's Republic of China*
[3]*Center for High Energy Physics, Peking University,*
No. 5 Yiheyuan Road, Beijing 100871, People's Republic of China
[4]*Collaborative Innovation Center of Quantum Matter,*
No. 5 Yiheyuan Road, Beijing 100871, People's Republic of China

In this work, we study the circular motions of charged particles and their polarized images around the Kerr black hole immersed in a weak magnetic field. We pay special attention to the case where the magnetic field and the charge-to-mass ratio are insignificant. Thus, the effective potential along the radial motion reduces to a cubic form approximately so that we can express the radius of the innermost stable circular orbit analytically in terms of the energy and angular momentum of charged particles. Moreover, we computed the polarized radiation of these particles and obtained the polarized images semianalytically for different spins, observational angles, and prograde and retrograde orbits. In particular, we find that these parameters significantly impact the polarization rotation and the magnitude of the polarization flux.

I. INTRODUCTION

Black holes are among the most fascinating predictions of general relativity, and accumulating evidence supports their existence in the Universe. Recent detections of gravitational waves by LIGO and Virgo [1–4] and imaging of black holes by the Event Horizon Telescope (EHT) Collaboration [5–10] have increased our confidence in the accuracy of general relativity and the existence of black holes. General relativity and other theories of gravity predict various types of black holes, including neutral, charged, magnetic, or both charged and magnetic. Astrophysical black holes are typically expected to be neutral, because they selectively accrete ambient matter. Despite this, these black holes can still generate a strong electromagnetic field that creates charged particles through pair production, as explained by Blandford and Znajek [11]. Furthermore, weakly charged black holes may exist in the Universe, and one possible mechanism for charging them is the accretion of free charged particles to neutralize the electric field generated by a rotating black hole immersed in a magnetic field [12].

The environment surrounding an astrophysical black hole is highly complex, containing plasma that generates magnetic fields and forms an accretion disk. Numerous observations have suggested the existence of magnetic fields outside black holes, including bright "flares," polarized broad Hα lines, and polarization of accretion disk radiation near active galactic nuclei [13–16]. Recently, the EHT Collaboration published a polarized image of the M87 black hole which provides further evidence of a magnetic field around the black hole [17–20], as is consistent with specific models of the magnetic field.

Studying the effects of the magnetic field around a black hole is crucial for interpreting information obtained from polarized images of the black hole. In this study, we are using a simplified model that disregards the interaction between charged particles and approximates their motions as pointlike. We then examine the polarized radiation resulting from the accelerated motion of the charged particle in a magnetic field, approximating it as electromagnetic radiation from point particles. Especially when the charged particles are in relativistic motion, the resulting radiation is commonly referred to as synchrotron radiation. Moreover, we assume that charged particles are confined to move in circular paths on the equatorial plane beyond the innermost stable circular orbit (ISCO). Factors such as the influence of the Lorentz force on charged particles' ISCOs and the polarized image of radiation in the presence of magnetic fields are essential. The ISCOs of charged particles around a Schwarzschild and Kerr black hole immersed in a weak, axially symmetric magnetic field

*Corresponding author.
minyongguo@bnu.edu.cn

have been widely studied, with many exciting results found [21–24]. For strong magnetic fields, spacetimes can be modeled by Schwarzschild and Kerr black holes that are embedded in the Melvin universe [25,26], and the corresponding ISCOs for massive particles have also been studied in the literature [27–29]. In addition, the polarized image of radiation originating from circularly orbiting charged particles acted upon by Lorentz force has been investigated in Schwarzschild and Kerr black holes with weak or strong magnetic fields [28,30–37].

In this work, we revisit the ISCOs of charged particles around a Kerr black hole with a weak magnetic field, originally discovered by Wald in Ref. [12]. In contrast to previous research, we focus on the case $\mathcal{B} = \frac{qB}{2m} \ll 1$, where q, m, and B are the charge, mass, and strength, respectively, of the magnetic field. This condition allows us to obtain an analytical expression for the radius of the ISCO that involves the energy E and angular momentum L of charged particles. As many astrophysical clouds of dust or fluids in our Universe do not have an extreme charge-mass ratio, the ubiquitous satisfaction of the $\mathcal{B} \ll 1$ condition makes our results useful in practical situations. In addition, we examine the polarized image of charged particles in circular motion on the equatorial plane observed by an observer at infinity. Unlike typical treatments of synchrotron radiation of a charged particle around a black hole, which rely on radiation study in the local inertial frame, we apply the covariant formulas of electromagnetic radiation that encode the intensity and polarization direction of radiation in curved spacetime. These formulas were recently developed in Ref. [36], building on earlier related discussions found in Ref. [38]. In addition, it is relevant to note that we have developed a simplified model in which charged particles move in circular orbits on the equatorial plane under the combined influence of gravity and Lorentz force, reminiscent of electrons in a ring accelerator. Such motion of charged particles in a magnetic field produces linearly polarized radiation, which becomes synchrotron radiation when the particles move relativistically [36]. However, when observing a black hole in a real astrophysical system, the EHT has observed synchrotron radiation originating from magnetic accretion flows [17–20]. Magnetic fluid is a plasma made up of charged particles and possesses a magnetic field. As these charged particles spiral within the magnetic field at relativistic speeds, they emit synchrotron radiation. Because of this difference, our simplified model cannot entirely account for the polarized images of black holes observed so far and, thus, is more suited for theoretical investigation. Nevertheless, if polarized radiation from charged particles can be directly observed, our model will become more applicable. Building on our simplified model, we demonstrate the polarization directions and total flux of the radiation emitted from charged particles for various spins, observational angles, and orbits. Our numerical studies on polarized images are not restricted

to the case $\mathcal{B} \ll 1$, although our primary focus is on researching ISCOs within this approximation.

The remaining parts of this paper are organized as follows. In Sec. II, we study the circular orbits of the charged particles around a Kerr black hole with a Wald magnetic field. In Sec. III, we review the electromagnetic radiation in curved spacetime [36] and calculate the polarized images of the charged particles in circular motions around a Kerr black hole. The main conclusions are summarized in Sec. IV. In this work, we have set the fundamental constants c, G, and the vacuum permittivity ε_0 to unity, and we will work in the signature convention $(-, +, +, +)$ for the spacetime metric.

II. CIRCULAR ORBITS OF A CHARGED PARTICLE AROUND A KERR BLACK HOLE WITH A WALD MAGNETIC FIELD

In this section, we focus on the circular orbits of a charged particle around a Kerr black hole with a Wald magnetic field.

A. Kerr black hole with a Wald magnetic field

The spacetime of a neutral and rotating black hole in general relativity is described by the Kerr black hole metric, which is a stationary and axisymmetric solution of the Einstein equations and takes

$$
\begin{aligned}
\mathrm{d}s^2 = {}& -\left(1 - \frac{2Mr}{\Sigma}\right)\mathrm{d}t^2 + \frac{\Sigma}{\Delta}\mathrm{d}r^2 + \Sigma\,\mathrm{d}\theta^2 \\
& + \left(r^2 + a^2 + \frac{2Mra^2}{\Sigma}\sin^2\theta\right)\mathrm{d}\phi^2 - \frac{4Mra}{\Sigma}\sin^2\theta\,\mathrm{d}t\,\mathrm{d}\phi
\end{aligned}
$$

(2.1)

in the Boyer-Lindquist coordinates, where

$$
\Sigma = r^2 + a^2\cos^2\theta, \qquad \Delta = r^2 - 2Mr + a^2, \quad (2.2)
$$

with M and a being the mass and spin of the Kerr black hole, respectively. And the angular momentum of the Kerr black hole is $J = Ma$. The horizons are located at $r_\pm = M \pm \sqrt{M^2 - a^2}$, given by the equation $\Delta = 0$. The outer one is the event horizon of the Kerr black hole, that is, $r_h = r_+$. Next, we assume that there is a vertical and uniform magnetic field outside the Kerr black hole, described by the Wald solution to the source-free Maxwell equations, that is, $\nabla_\mu F^{\mu\nu} = 0$. The magnetic field is aligned with the rotation axis of the black hole and independent of the coordinates t and ϕ. Considering the two Killing vectors $\eta^a = (\frac{\partial}{\partial t})^a$ and $\psi^a = (\frac{\partial}{\partial \phi})^a$, Wald proved that the field

$$
A^a = \frac{1}{2}B\left(\psi^a + \frac{2J}{M}\eta^a\right) - \frac{Q}{2M}\eta^a \qquad (2.3)
$$

gives a unique field that is an asymptotically uniform magnetic field of strength B_0, with Q being the charge of the Kerr black hole. Next, we introduce the electrostatic injection energy, defined as the difference between the electric potential at the horizon and infinity, i.e.,

$$\epsilon = eA_\mu\eta^\mu|_{\text{horizon}} - eA_\mu\eta^\mu|_\infty, \qquad (2.4)$$

which is a constant over the black hole [12]. For a pure Kerr spacetime, we should have $Q = 0$. However, due to non-vanishing electrostatic injection energy ϵ, an electric field is induced by the rotation of the black hole in the presence of the magnetic field. It causes charged particles to be attracted by the black hole, a process called charged accretion. As a result, to reach a steady state, the black hole has to gain a nonzero net charge to reach equilibrium, that is, $\epsilon = 0$, which gives

$$Q = 2BJ. \qquad (2.5)$$

In the following, we focus mainly on this equilibrium situation. Note that, in Ref. [39], they also paid attention to the nonequilibrium situations. It is worth mentioning that Eq. (2.5) holds for an arbitrary stationary, axisymmetric black hole; that is, the condition is not limited to Kerr black holes. In principle, the charge and magnetic field would react upon the background spacetime. If we want to ignore the contribution of the magnetic field to the background spacetime for simplicity, we need to consider the weak field approximation:

$$BM \ll 1. \qquad (2.6)$$

On the other hand, the characteristic length scale given by the charge of the black hole is comparable with the gravitational radius when

$$\sqrt{\frac{Q_G^2 G}{c^4}} = \frac{2GM}{c^2}, \qquad (2.7)$$

so that the gravitational effect of the charge Q on the background can be ignored if

$$Q \ll Q_G. \qquad (2.8)$$

Note that we have restored G and c in Eq. (2.7), making the physical meaning of the formula more explicit. In addition, considering $J \le M^2$, from Eq. (2.5) we have

$$\frac{Q}{Q_G} = \frac{Q}{2M} = Ba \le BM \ll 1, \qquad (2.9)$$

which means we are allowed to omit the charge's influence on the spacetime metric, although there is a nonzero net

charge so that we can stick to the Kerr metric under the weak field approximation. In fact, in the Gauss units, we find

$$B_{\text{Gauss}} = \frac{c^4}{G^{3/2}M}(BM) \simeq 2.36 \times 10^{19} \frac{M_\odot}{M}(BM) \text{ G}. \qquad (2.10)$$

Here, (BM) is a dimensionless number and can also be seen as the value of B in our simplified unit after setting c, G, ϵ_0, and M to 1, and $M_\odot$ is the mass of the Sun. For supermassive black holes $M \sim 10^9 M_\odot$, the dimensionless $BM = 0.01 \ll 1$ corresponds to $B_{\text{Gauss}} \sim 10^8$ G, which is already a very significant value for an astrophysically appropriate magnetic field around an astronomical black hole. Thus, the weak field approximation $BM \ll 1$ can be imposed for most real astronomical black holes with magnetic fields and deserves careful study.

B. Motions of charged particles on the equatorial plane

In this subsection, we move to study the motions of charged particles on the equatorial plane under the weak field approximation employing the standard approach. In the Boyer-Lindquist coordinates, the generalized four-momentum P^μ can be written as

$$P^\mu = p^\mu + qA^\mu, \qquad (2.11)$$

where $p^\mu = mu^\mu$ is the four-momentum for the charged particle with m being the mass, A^μ is the electric vector potential, and q is the charge of the particle. From Eq. (2.3), we have

$$A^\mu = \left(aB - \frac{Q}{2M}, 0, 0, \frac{B}{2}\right). \qquad (2.12)$$

Note that the Lie derivatives of A_μ with respect to the Killing vectors η^μ and ψ^μ are zero, that is,

$$\mathcal{L}_\eta A_\mu = 0, \qquad \mathcal{L}_\psi A_\mu = 0, \qquad (2.13)$$

and, thus, we can construct two conserved quantities along the motions of charged particles:

$$E = -\frac{P^\mu}{m}g_{\mu\nu}\eta^\nu = -P_t/m,$$
$$L = \frac{P^\mu}{m}g_{\mu\nu}\psi^\nu = P_\phi/m. \qquad (2.14)$$

Note that the energy can be explicitly written out as

$$E = \left(1 - \frac{2Mr}{\Sigma}\right)\left[\frac{q(aB - \frac{Q}{2M})}{m} + \frac{dt}{d\tau}\right] + \frac{aMr\sin^2\theta(Bq + 2m\frac{d\phi}{d\tau})}{m\Sigma}, \qquad (2.15)$$
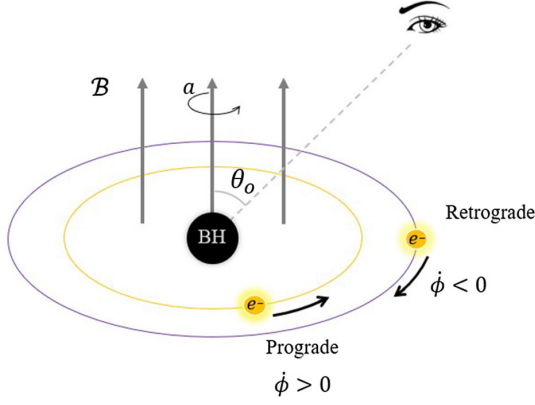
FIG. 1.   A diagram of charged particles moving in circular orbits on the equatorial plane of the Kerr spacetime with a vertical and uniform magnetic field. We assume that the spin of the Kerr black hole and the magnetic field are in the same direction when a and $\mathcal{B}$ have the same sign.

so it is not necessarily positive. Similarly, L would not be necessarily positive even if $\frac{\partial \phi}{\partial \tau} > 0$.

Since we are interested in the circular motions confined to the equatorial plane as illustrated in Fig. 1, the four-velocity of the charged particle takes

$$u^\mu = (\dot{t}, \dot{r}, 0, \dot{\phi}), \qquad (2.16)$$

where "˙" denotes derivative with respect to the proper time τ. From Eq. (2.14), we can obtain

$$\frac{dt}{d\tau} = \frac{g_{\phi\phi}(E + \frac{q}{m}A_t) + g_{t\phi}(L - \frac{q}{m}A_\phi)}{g_{t\phi}^2 - g_{tt}g_{\phi\phi}}, \qquad (2.17)$$

$$\frac{d\phi}{d\tau} = \frac{g_{tt}(-L + \frac{q}{m}A_t) + g_{t\phi}(-E - \frac{q}{m}A_t)}{g_{t\phi}^2 - g_{tt}g_{\phi\phi}}. \qquad (2.18)$$

Note that the four-velocity of a charged particle is future directed; thus, we have $\dot{t} > 0$, which gives us

$$E > \frac{2aL}{r^3 + a^2 r + 2a^2}, \qquad (2.19)$$

where we have used the equilibrium condition, that is, $Q = 2BJ$, and set the mass of the black hole $M = 1$ here and hereafter. Moreover, the four-velocity of the charged particle is normalized, that is, $u^\mu u_\mu = -1$. Then, combining Eq. (2.14) and the normalization condition of the four-velocity, we can obtain

$$\dot{r}^2 + V_{\rm eff} = 0, \qquad (2.20)$$

where we have defined the effective potential $V_{\rm eff}$ as

$$V_{\rm eff} = \frac{\mathcal{B}^2 \Delta (a^2 r + r^3 + 2a^2) - 2Lr\Delta\mathcal{B} - (2a^2 + a^2 r + r^3)E^2 + 4aLE + r\Delta - 2L^2 + L^2 r}{r^3}. \qquad (2.21)$$

Here, we have introduced a new parameter

$$\mathcal{B} = \frac{qB}{2m}. \qquad (2.22)$$

It can be explicitly written as $V_{\rm eff} = \frac{P_5(r)}{r^3}$, where $P_5(r)$ is a fifth-order polynomial of r. To write out the coefficients explicitly, we have

$$P_5(r) = c_5 r^5 + c_4 r^4 + c_3 r^3 + c_2 r^2 + c_1 r + c_0,$$
$$c_0 = -2(L - aE)^2 + 2a^4 \mathcal{B}^2,$$
$$c_1 = a^2 + (-4a^2 + a^4)\mathcal{B}^2 - 2a^2 \mathcal{B}L + L^2 - a^2 E^2,$$
$$c_2 = -2 + 4\mathcal{B}L, \qquad c_3 = 1 + 2a^2 \mathcal{B}^2 - 2\mathcal{B}L - E^2,$$
$$c_4 = -2\mathcal{B}^2, \qquad c_5 = 2\mathcal{B}^2. \qquad (2.23)$$

In addition, it will useful to evaluate $V_{\rm eff}$ at the horizon $x = \frac{1}{r_h}$, and the result reads

$$-r_+^3 V_{\rm eff}(r = r_h) = 4E^2 r_+ + L^2 r_- - 4aEL. \qquad (2.24)$$

Here, the terms regarding $\mathcal{B}$ have become zero. This also implies that, around the horizon, the impact of the magnetic field on particles would become small. Also,

$$4E^2 r_+ + L^2 r_- - 4aEL \geq 2\sqrt{4E^2 L^2 r_+ r_-} - 4aEL = 0; \qquad (2.25)$$

therefore, we can see that the effective potential is always non-negative at the horizon. The equation holds if and only if $4E^2 r_+ = L^2 r_-$, which gives $\frac{L}{E} = \pm \frac{2r_+}{a}$.

C. Circular orbits of charged particles

Next, we turn to calculate the circular orbits of charged particles in the Kerr spacetime with a Wald magnetic field. For simplicity, we set $\mathcal{B} > 0$ and let the spin a vary from -1 to 1. To find the energy E and angular momentum L at a radius r, we need to solve the following equations:

$$V_{\rm eff} = 0 \quad \text{and} \quad \partial_r V_{\rm eff} = 0, \qquad (2.26)$$

and the ISCO can be determined by further requiring

$$\partial_r^2 V_{\mathrm{eff}} = 0. \qquad (2.27)$$

It is easy to see that $V_{\mathrm{eff}} = 0$ can be reduced to a quintic equation for r, which cannot generally be solved analytically. And, thus, one has to solve Eqs (2.26) and (2.27) numerically to gain insights into the ISCOs of charged particles in the Kerr spacetime with a Wald magnetic field; see examples in Ref. [39].

However, one can see that $V_{\mathrm{eff}} = 0$ reduces to a cubic equation for r if the term including $\mathcal{B}^2$ can be dropped, which is legal when $\mathcal{B} \ll 1$. Considering that a cubic equation can be solved analytically and an analytical expression is useful for better understanding the circular orbits of charged particles in the Kerr spacetime with a Wald magnetic field, we carefully study the case $\mathcal{B} \ll 1$. Let us start by discussing when the approximate condition holds in the Gauss units. Note that, in the present convention, $\mathcal{B} = k$ means $\mathcal{B} = kM^{-1}$, where k is a dimensionless number; we can recover the full expression of $\mathcal{B} = k$ in the Gauss units:

$$\left(\frac{qB}{2m}\right)_{\mathrm{Gauss}} = k\frac{c^4}{GM}, \qquad (2.28)$$

and this gives

$$\left(\frac{q}{e}\right)\left(\frac{m_p}{m}\right) = \frac{43}{B_{\mathrm{Gauss}}}\frac{M_\odot}{M}k = 1.8 \times 10^{-18}\frac{(\mathcal{B}M)}{(BM)}, \qquad (2.29)$$

where m_p is the proton mass, e is the unit charge, and we have plunged Eq. (2.10) in the last "= ." Thus, the approximate condition $\mathcal{B} \ll 1$ corresponds to

$$\left(\frac{q}{e}\right)\left(\frac{m_p}{m}\right)(BM) \ll 1.8 \times 10^{-18}. \qquad (2.30)$$

As a result, we can see that the approximate condition $\mathcal{B} \ll 1$ is applicable for an object with a unit charge whose mass is much larger than $10^{18}(BM)m_p$. For example, from Eq. (2.10), we find $BM = 10^{-9}$ if we consider a supermassive black hole with $M \sim 10^9 M_\odot$ immersed in a magnetic field with $B = 10$ G, then the mass of the object with a unit charge should be much larger than $m = 10^9 m_p = 10^{-18}$ kg in the international system of units if we require that the approximate condition $\mathcal{B} \ll 1$ holds in our present convention. To be precise, the charge-to-mass ratio of an electron is 1.7×10^{11}, which is too extreme for our approximation in Eq. (2.30), as an electron would have $\mathcal{B} = 8.6 \times 10^{10}$. However, the charge-to-mass ratio of ionized gas molecules is much lower, ranging from 10^6 to 10^8, making it easier to satisfy the approximation condition $\mathcal{B} \ll 1$. This approximation is particularly helpful for studying charged astrophysical dust clouds and weakly magnetized black holes with low mass.

Now, we move to study the orbits of charged particles in the case $\mathcal{B} \ll 1$. We dropped the second-order terms for $\mathcal{B}$ in the effective potential, and Eq. (2.21) can be simplified as

$$-V_{\mathrm{eff}} = 2(L - 2aE)^2 x^3 + (-a^2 + 2a^2\mathcal{B}L - L^2 + a^2E^2)x^2 \\ + (2 - 4\mathcal{B}L)x + E^2 + 2\mathcal{B}L - 1, \qquad (2.31)$$

where a new parameter $x = 1/r$ is introduced for simplicity. The equations for a circular orbit

$$V_{\mathrm{eff}} = \partial_r V_{\mathrm{eff}} = \partial_r^2 V_{\mathrm{eff}} = 0 \qquad (2.32)$$

correspond to the equations

$$V_{\mathrm{eff}} = \partial_x V_{\mathrm{eff}} = \partial_x^2 V_{\mathrm{eff}} = 0. \qquad (2.33)$$

This would be true except for two points: $r = 0$ inside the horizon and $r = \infty$, so we can obtain the ISCOs by solving Eq. (2.33).

In the following subsections, we will analyze the effective potential's form and root structures under this approximation.

1. Quadratic form

Next, let us begin with the first equation, $V_{\mathrm{eff}} = 0$. It is easy to see that the cubic equation is simplified into a quadratic equation when $L = aE$. Then, the effective potential function becomes

$$-V_{\mathrm{eff}} = (-1 + 2\mathcal{B}L)a^2 x^2 + 2(1 - 2\mathcal{B}L)x + E^2 + 2\mathcal{B}L - 1 \qquad (2.34)$$

$$= (-1 + 2\mathcal{B}L)\left(ax - \frac{1}{a}\right)^2 + E^2 + (2\mathcal{B}L - 1)\left(1 + \frac{1}{a^2}\right). \qquad (2.35)$$

When $-1 + 2\mathcal{B}L = 0$, that is, $L = \frac{1}{2\mathcal{B}}$, we find $V_{\mathrm{eff}} = -E^2$, which implies no stable circular orbits of charged particles exist in this situation.

When $-1 + 2\mathcal{B}L > 0$, we find

$$-V_{\mathrm{eff}}(x = 0) = E^2 + 2\mathcal{B}L - 1 > 0,$$

$$-V_{\mathrm{eff}}\left(x = \frac{1}{r_+}\right) > 0, \qquad \frac{1}{a^2} \geq 1 \geq \frac{1}{r_+}, \qquad (2.36)$$

so that $-V_{\mathrm{eff}}$ is a monotonic decreasing function and $-V_{\mathrm{eff}} > 0$ is always true in the region $x \in (0, 1/r_+)$, which implies there are no circular orbits of charged particles.

At last, we focus on the case $2\mathcal{B}L - 1 < 0$. In addition, combining Eq. (2.19) with $L = aE$, we can find the energy satisfies

$$0 < E < \frac{1}{2\mathcal{B}a} \quad \text{with} \quad 0 < a \leq 1; \tag{2.37}$$

thus, we can obtain

$$-1 < -V_{\text{eff}}(x = 0) = E^2 + 2\mathcal{B}aE - 1 < \frac{1}{4\mathcal{B}^2 a^2}. \tag{2.38}$$

On the other hand, we find $-V_{\text{eff}}$ is a monotonic increasing function in the region $x \in (0, 1/r_+)$ in the case $2\mathcal{B}L - 1 < 0$, and so

$$-V_{\text{eff}}(x = 0) < -V_{\text{eff}} < -V_{\text{eff}}(x = 1/r_+) \tag{2.39}$$

in the region $x \in (0, 1/r_+)$. Thus, when $0 < E < \sqrt{1 + a^2\mathcal{B}^2} - a^2\mathcal{B}^2$, we have $-V_{\text{eff}}(x = 0) < 0$ and there must be a r_0 such that $V_{\text{eff}}(r_0) = 0$. This implies there is a forbidden zone $(r_0, +\infty)$ for charged particles when $0 < E < \sqrt{1 + a^2\mathcal{B}^2} - a^2\mathcal{B}^2$. When $\sqrt{1 + a^2\mathcal{B}^2} - a^2\mathcal{B}^2 \leq E < \frac{1}{2\mathcal{B}a}$, we have $-V_{\text{eff}}(x = 0) > 0$ and there is no forbidden zone for charged particles. In both cases, there are no circular orbits for charged particles.

In conclusion, now we can ensure that there are no circular orbits for charged particles when $L = aE$.

2. Cubic form

Then let us pay attention to the more general situation in which $L \neq aE$ and the effective potential function is cubic. To investigate the structure of the potential, it is convenient to define a new variable y by

$$x = y + \frac{d}{3\tilde{a}}, \tag{2.40}$$

where we set

$$d = L^2 + a^2(1 - 2\mathcal{B}L - E^2),$$
$$\tilde{a} = 2(L - aE)^2, \tag{2.41}$$

and then we get a compact form

$$f(y) = -V_{\text{eff}} = \tilde{a}y^3 + by + c, \tag{2.42}$$

where

$$b = 2 - 4\mathcal{B}L - \frac{d^2}{3\tilde{a}},$$
$$c = -1 + 2\mathcal{B}L + E^2 + \frac{2(1 - 2\mathcal{B}L)d}{3\tilde{a}} + \frac{d^3}{27\tilde{a}}. \tag{2.43}$$

Then, we find

$$-\partial_x V_{\text{eff}}(x) = \partial_y f(y) = 3\tilde{a}t^2 + b. \tag{2.44}$$

A circular orbit has to satisfy $\partial_x V_{\text{eff}}(x) = 0$, such that we have $b < 0$ since $\tilde{a}$ is always positive. Furthermore, $y = \sqrt{\frac{-b}{3\tilde{a}}}$ gives us a local maximum of the effective potential V_{eff}, while $y = -\sqrt{\frac{-b}{3\tilde{a}}}$ corresponds to a local maximum. Then the necessary and sufficient conditions for the existence of a future-directed stable circular orbit are

$$0 < y_0 = \sqrt{\frac{-b}{3\tilde{a}}} + \frac{d}{3\tilde{a}} < \frac{1}{r_+} \tag{2.45}$$

and

$$f\left(\sqrt{\frac{-b}{3\tilde{a}}}\right) = 0, \tag{2.46}$$

as well as Eq. (2.19). In addition, the condition $f(\sqrt{\frac{-b}{3\tilde{a}}}) = 0$ is equivalent to

$$\frac{c^2}{4} + \frac{b^3}{27\tilde{a}} = 0, \tag{2.47}$$

which gives a constraint for the conserved quantities L and E. That is to say, when Eqs. (2.45), (2.47), and (2.19) hold, a stable future-directed circular orbit for a charged particle must exist, and the radius is given by

$$r_0 = 1/y_0, \tag{2.48}$$

where y_0 is given in Eq. (2.45).

We can push our calculations to determine the ISCO of the charged particle. Considering the equation $\partial_x^2 V_{\text{eff}}(x) = \partial_y^2 f(y) = 0$, we can easily find the following conditions:

$$b = c = 0, \tag{2.49}$$

$$r_{\text{ISCO}} = 1/y_{\text{ISCO}} = \frac{3\tilde{a}}{d} = \frac{6(L - aE)^2}{a^2 - 2a^2\mathcal{B}L + L^2 - a^2E^2} \tag{2.50}$$

are true if there is an ISCO of the charged particle on the equatorial plane in the Kerr spacetime with a weak magnetic field under the approximate condition $\mathcal{B} \ll 1$. Here, it is worth emphasizing that the energy E and angular momentum L can be obtained by solving Eq. (2.49), and then Eq. (2.50) can give us the value of the radius of the ISCO. While, for $\mathcal{B} \gg 1$ and $\mathcal{B} \sim \mathcal{O}(1)$, we have to obtain the ISCO and orbits of charged particles numerically. Note that, in numerical calculations, we can use the

fact that if Eqs. (2.26) and (2.27) hold, then the fifth-order polynomial (2.23) that we mentioned should also satisfy

$$P_5(r) = 0, \qquad \partial_r P_5(r) = 0, \qquad (2.51)$$

which will greatly simplify the computation.

III. POLARIZED IMAGES OF CHARGED PARTICLES IN CIRCULAR ORBITS

In this section, we move to study polarized images of charged particles that move in circular motions on the equatorial plane of the Kerr spacetime with a Wald magnetic field. The observer is located at infinity with an inclination angle θ_o as shown in Fig. 1.

A. Polarization of electromagnetic radiation and propagation of light

In this subsection, we introduce the necessary formulas to calculate the polarization of electromagnetic radiation originating from the charged particle and propagation of light following our previous work [36]. When charged particles are affected by Lorentz forces, they are obliged to move in nongeodesic trajectories and generate electromagnetic radiation with nice polarization properties. The polarization vector of the electromagnetic radiation takes

$$f^\mu = N^{-1}[\delta^\mu_\alpha(k_\beta D_\tau u^{[\beta} u^{\alpha]})], \qquad (3.1)$$

where u^α has been introduced to be the four-velocity of the charged particle in the last section, k_β is the wave vector of the polarized radiation and normalized by $k^\beta u_\beta = 1$, D_τ is derivative operator along the vector u^β, that is, $D_\tau \equiv u^\alpha \nabla_\alpha$ with τ being the proper time of u^α, and N^{-1} is a normalization factor in ensuring $f_\mu f^\mu = 1$. In addition, the luminosity of the polarized radiation is given by

$$L = 4\pi |k_\beta D_\tau u^\beta u^\alpha - D_\tau u^\alpha|^2. \qquad (3.2)$$

Next, we consider the photon's position that hits the observer's screen with coordinates $(t_o, r_o, \theta_o, \phi_o)$. In terms of celestial coordinates, the position can be described by

$$\alpha = -\frac{\lambda}{\sin\theta_o}, \qquad \beta = \pm_o\sqrt{\Theta(\theta_o)}, \qquad (3.3)$$

where $\pm_o = \mathrm{sgn}(k^\theta_o)$ represents the sign of k^θ in the observer's frame and $\lambda = l/\omega$ is an impact parameter with l and ω being the angular momentum and energy of the photon, respectively. $\Theta(\theta)$ is the angular potential of the photon, which reads

$$\Theta(\theta) = \eta + a^2\cos^2\theta - \lambda^2\cot^2\theta, \qquad (3.4)$$

where $\eta = \mathcal{Q}/\omega^2$ is the other impact parameter with $\mathcal{Q}$ being the Carter constant in the Kerr spacetime. On the other hand, charged particles as the light source are located on the equatorial plane with coordinates $(t_s, r_s, \pi/2, \phi_s)$. In principle, with the help of null geodesic equations in Kerr spacetime, one can obtain the trajectories of photons connecting the source and the observer, and then we can find the images of the source; that is, we know the coordinates (α, β) on the screen of the observer. We want to stress that there is more than one trajectory of lights starting at the source and ending at the observer, since the lights may turn around the black hole more than once before reaching the observer. We use m to denote the number of times the trajectory crosses the equatorial plane between the source and the observer; different values of m correspond to the $(m+1)$th image on the observers' screen. In particular, the image formed by the trajectories with $m = 0$ is often called the primary image, the image with $m = 1$ is called the secondary image, and so on. For more details, one is suggested to refer to Ref. [40].

Furthermore, we also need to obtain the polarization information of the image. Following Ref. [36], the polarization information can be transmitted from the source to the observer by using the Penrose-Walker (PW) constant

$$\kappa = 2k^\mu f^\nu(\hat{l}_{[\mu}\hat{n}_{\nu]} - \hat{m}_{[\mu}\hat{\bar{m}}_{\nu]})(r - ia\cos\theta) \equiv \omega(\kappa_1 + i\kappa_2), \qquad (3.5)$$

which is a conserved quantity along the null geodesics for Kerr spacetime. In the above formula, $\kappa_{1,2}$ are the rescaled real and imaginary parts of the PW constant, respectively. And $\hat{l}, \hat{n}, \hat{m},$ and $\hat{\bar{m}}$ are the Neumann-Penrose tetrads which can be chosen as

$$\hat{l} = \frac{1}{\sqrt{2\Delta\Sigma}}[(r^2 + a^2)\partial_t + \Delta\partial_r + a\partial_\phi],$$

$$\hat{n} = \frac{1}{\sqrt{2\Delta\Sigma}}[(r^2 + a^2)\partial_t - \Delta\partial_r + a\partial_\phi],$$

$$\hat{m} = \frac{1}{\sqrt{2}(r + ia\cos\theta)}\left(ia\sin\theta\partial_t + \partial_\theta + \frac{i}{\sin\theta}\partial_\phi\right),$$

$$\hat{\bar{m}} = \frac{1}{\sqrt{2}(r - ia\cos\theta)}\left(-ia\sin\theta\partial_t + \partial_\theta + \frac{i}{\sin\theta}\partial_\phi\right). \qquad (3.6)$$

Thus, employing Eq. (3.5), at the observer, we can decode the information of f^μ given at the source, and on the polarization, the vector can be read from the PW constant as

$$\vec{\mathcal{E}} = (\mathcal{E}_\alpha, \mathcal{E}_\beta) = \frac{1}{\omega(\beta^2 + \gamma^2)}(\beta\kappa_2 - \gamma\kappa_1, \beta\kappa_1 + \gamma\kappa_2),$$

$$\gamma = -(\alpha + a\sin\theta_o). \qquad (3.7)$$

On the other hand, we still need to know the total fluxes of the image considering charged particles have a finite size. We omit the details and give the result of the total fluxes instead, which takes

$$F_o = \frac{g^4 L}{4\pi r_o^2 |\hat{k}| \cdot X} \left| \frac{\partial(\alpha, \beta)}{\partial(Y_s, Z_s)} \right|, \tag{3.8}$$

where $\left| \frac{\partial(\alpha,\beta)}{\partial(Y_s,Z_s)} \right|$ denotes the Jacobian determinant between the coordinates (α, β) and (Y_s, Z_s). Thereinto, (Y_s, Z_s) are coordinates defined on the "source screen" with $T = X = 0$. $\{T, X, Y, Z\}$ is a local Minkowski coordinate system in the neighborhood of the source, which is defined as

$$T e_{(t)} + X e_{(r)} + Y e_{(\phi)} - Z e_{(\theta)} = (x^\mu - x_*^\mu)\partial_\mu, \tag{3.9}$$

where x_*^μ are the coordinates of the source and $e_{(\mu)}$ are the tetrad of the source. For a Kerr metric, we choose

$$e_{(t)} = \gamma \sqrt{\frac{\Xi}{\Delta\Sigma}}(\partial_t + \Omega_s \partial_\phi), \quad e_{(r)} = \frac{\Delta}{\Sigma}\partial_r, \quad e_{(\theta)} = \frac{1}{\sqrt{\Sigma}}\partial_\theta,$$

$$e_{(\phi)} = \gamma v_s \sqrt{\frac{\Xi}{\Delta\Sigma}}\left[\partial_t + \frac{2aMr}{\Xi}\right] + \gamma\sqrt{\frac{\Sigma}{\Xi}}, \tag{3.10}$$

where we have introduced

$$\Xi = (r^2 + a^2)^2 - \Delta a^2 \sin^2\theta \tag{3.11}$$

and

$$v_s = \frac{\Xi}{\Sigma\sqrt{\Delta}}\left(\Omega_s - \frac{2aMr}{\Xi}\right), \qquad \gamma = \frac{1}{\sqrt{1 - v_s^2}}, \tag{3.12}$$

with $\Omega_s = \frac{d\phi_s}{dt_s}$ being the angular velocity of the source. In addition, the unit vector $\hat{k}$ is given by

$$\hat{k} = \frac{1}{k^{(t)}}(k^{(r)}X + k^{(\phi)}Y - k^{(\theta)}Z), \tag{3.13}$$

and g is the redshift factor which is given by

$$g = \frac{\omega_o}{\omega_s}, \tag{3.14}$$

where $\omega_{o,s}$ are the frequencies of the photon in the observer and the source frame, respectively. Now, we are ready to calculate some specific polarized images of charged particles orbiting the Kerr black hole with a Wald magnetic field.

B. Results

Based on our model, in this subsection, we show some results for our calculations with the observation angle at $\theta_o = 17°$ and $\theta_o = 80°$. In our computations of the polarized images, we use the full form of the effective potential to numerically determine the parameters for stable circular orbits without approximation. According to the previous analysis, when $\mathcal{B}$ and a are given, only one degree of freedom is left among r, E, and L for stable circular orbits. In our following calculations, we usually set $r_s = 6$ and compare the results with other different parameters; that is, we fix the radius of the orbit for charged particles and discuss the influence of the other parameters. The reason why we choose $r_s = 6$ is that the ISCO for a neutral particle in a Schwarzschild black hole spacetime is at $r_s = 6$, and we still hope to focus on polarized images of the source in this region. Our main interest is in the effects of the spin a, the observational angle θ_o on the polarized images, and the difference between the retrograde or prograde orbiting source.[1] In the following studies, we will vary a and θ_o and make plots in retrograde or prograde cases. In addition, as pointed out in Ref. [36], empirically, the strength of $\mathcal{B}$ does not affect the direction of the polarization vector f^μ and changes only the overall intensity of flux. It is also the case with Kerr spacetime. So we also fix $\mathcal{B} = 2$ in our work.

At first, we look at the difference in the polarized images between the prograde and retrograde orbits. We fix $a = 0.94$, which is a potential value of the spin of the supermassive black hole in M87 predicted by EHT [5–9]. The results are shown in Fig. 2, in which blue circles are the images of charged particles and red lines denote the polarization directions and total flux with the length. From Fig. 2, one can see that, for the prograde case in the left panel, there is barely any difference between the lengths of red lines on the left and right sides. However, for the retrograde case in the right panel in Fig. 2, we can find that the fluxes are much stronger on the right side than those on the left side. The main reason for this phenomenon is the so-called Doppler beaming (sometimes called the headlight effect). The radiation from moving particles concentrates upon the vicinity along the direction of the motion of particles, which becomes more significant when the velocity of moving particles is higher. Qualitatively, when $\mathcal{B}$ and L are in opposite directions, charged particles would have higher energies to stay in a circular orbit, so that the Doppler beaming is more substantial in the retrograde case. In addition, we can infer that the phenomenon would be more distinct when the observer is closer to the equatorial plane.

---

[1]Note that prograde (retrograde) is defined by $\dot\phi > 0$ ($\dot\phi < 0$) instead of $L > 0$ ($L < 0$), since the sign of the angular momentum L is not necessarily as same as the sign of $\dot\phi$, when there is an external magnetic field.
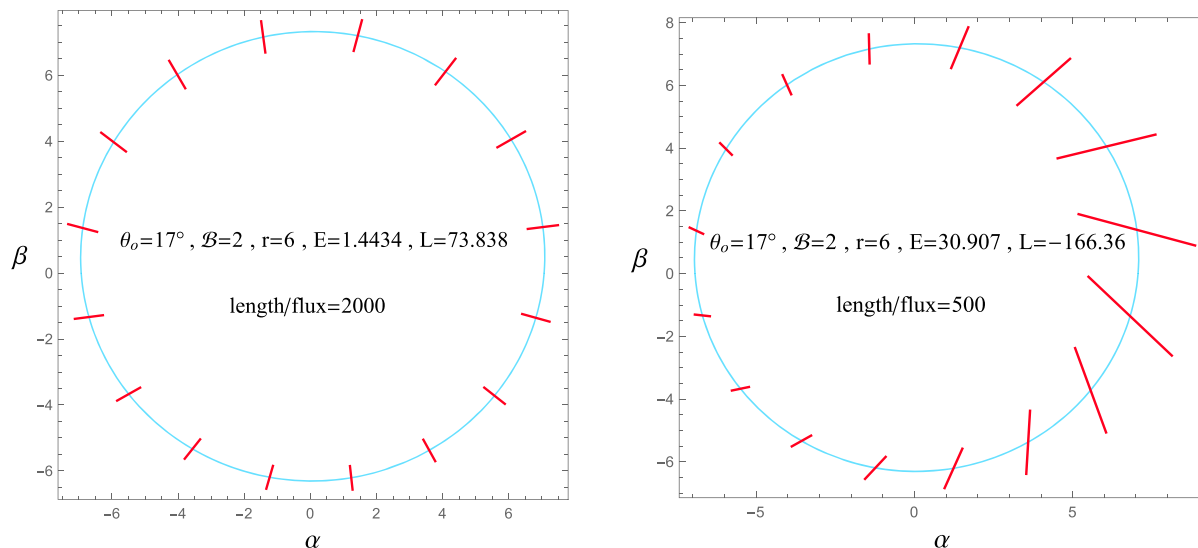
FIG. 2. Comparisons of polarized images between the prograde and retrograde orbits with $\theta_o = 17°$, $a = 0.94$, $r_s = 6$, and $\mathcal{B} = 2$. The left plot is for prograde orbit, while the right is retrograde. The corresponding energy E and angular momentum L for stable circular orbits are also shown in each plot. Blue circles give shapes of the images of charged particles, and red lines denote polarization information. In particular, the length of the red line signifies the magnitude of the total flux. Note that the lengths of the flux are scaled differently to make the lengths of lines in the two plots of the same order of magnitude.

Next, we turn to study the influence of the spin on the polarized images. In Fig. 3, we fix $\theta_o = 17°$ and $r_s = 6$ and vary a for retrograde orbits. The length ratio to the flux is 200 for the five plots. We can see evident changes in the magnitude of the flux, while the corresponding polarized directions show no significant changes as the spin a increases. In addition, we also checked the prograde orbits and found that, when we vary a, the changes in polarization and intensity are minor. Hence, we do not wish to present these results here.

Now we move on to the case that the observational angle is fixed at $\theta_o = 80°$, that is, the observer is close to the equatorial plane, and the spin a is varied from -0.99 to 0.99. The images of orbits deviate from circles a lot in this case. The results for the prograde case are shown in Fig. 4, where we have scaled the length of the polarization flux by length/flux = 4000. From the plot with $a = 0$, it seems that the polarizations of both sides centered on $\alpha = 0$ are approximately symmetric, which means that the Doppler beaming is not apparent. However, there is a significant difference in the flux between the upper and lower parts of the plot, which is caused by the curvature of the strongly curved spacetime. Meanwhile, at the top of the orbit, where $\alpha = 0$, the flux of the polarization is much smaller than those in neighboring places. The reason is that the position $(\alpha = 0, \beta = \beta_{\max})$ on the screen corresponds to the lights that radiate from the source with the four-momentum perpendicular to the velocity of charged particles in the local frame of the source, and they are much weaker than radiation going in other directions. This phenomenon can usually be observed when θ_o is bigger. Moreover, the spin

of the Kerr black hole also significantly impacts the image. When a is positive, the right side of the image is brighter than the left side and vice versa.

The results for the retrograde case are shown in Fig. 5, where we let $\theta_o = 80°$, $r = 6$, and $\mathcal{B} = 2$ and the spin a go from -0.99 to 0.99. In this case, one of the most obvious phenomena is that the Doppler effect is powerful, because the observational angle θ_o and the energy of the charged particles E are large. Thus, for the sake of visualization, we take a logarithm of the flux for the plots. In addition, the right side of the plot, where the particle moves toward the observer, has much stronger radiation. Also, in this case, the black hole spin a has a much larger impact on the polarization. Furthermore, in these plots, we can see a pronounced clockwise rotation of the polarizations as the spin a increases, while this rotation is unapparent for prograde orbits. Besides, we also find that this rotation happens but it is minimal for both prograde and retrograde orbits when θ_o is small such as $\theta_o = 17°$.

It is noteworthy that, in actual observations, the detectors or telescopes can detect electromagnetic radiation of only a certain frequency range. Therefore, let us make an estimation of the frequency of the particle moving on the ISCO. When discussing Kerr black holes, the velocity of the particles on the ISCO increases with the spin parameter a. In the case of a near extreme Kerr black hole, the particle velocity approaches the speed of light c on the ISCO, with the radius of the orbit only slightly larger than the black hole mass, that is, $r_{\text{ISCO}} \sim M$ [41]. In the international system of units, we have
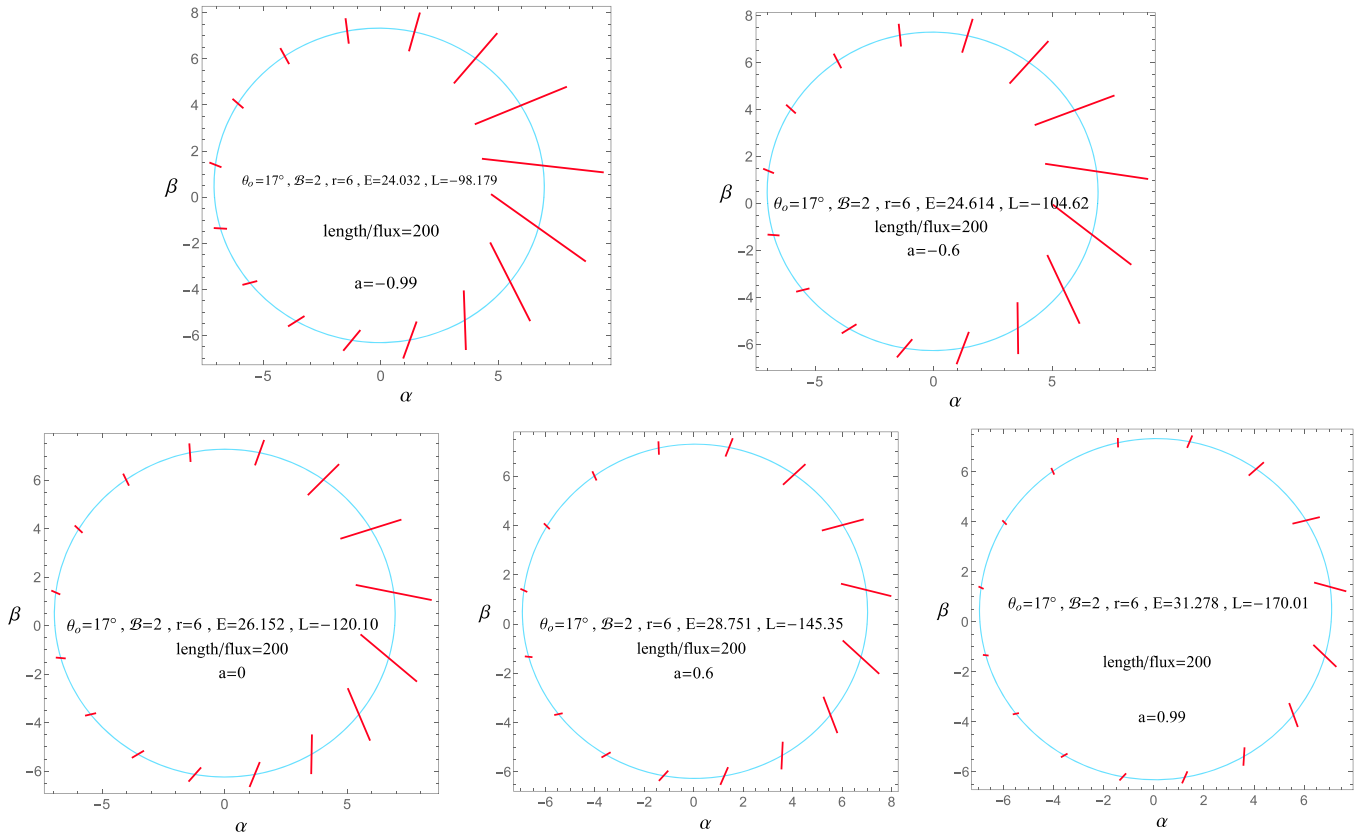
FIG. 3.   Polarized images of charged particles in retrograde orbits are produced with $\theta_o = 17°$, $\mathcal{B} = 2$, and $r_s = 6$. We let the spin a vary from -0.99 to 0.99. The energy E and the angular momentum L are directly calculated from the conditions of the stable circular orbit. Blue lines show the shapes of the images of the stable orbits. The inclinations of red lines denote the polarization directions of radiation, while the lengths represent the total flux. In this set of plots, we set length/flux = 4000 to make the plots more ornamental.

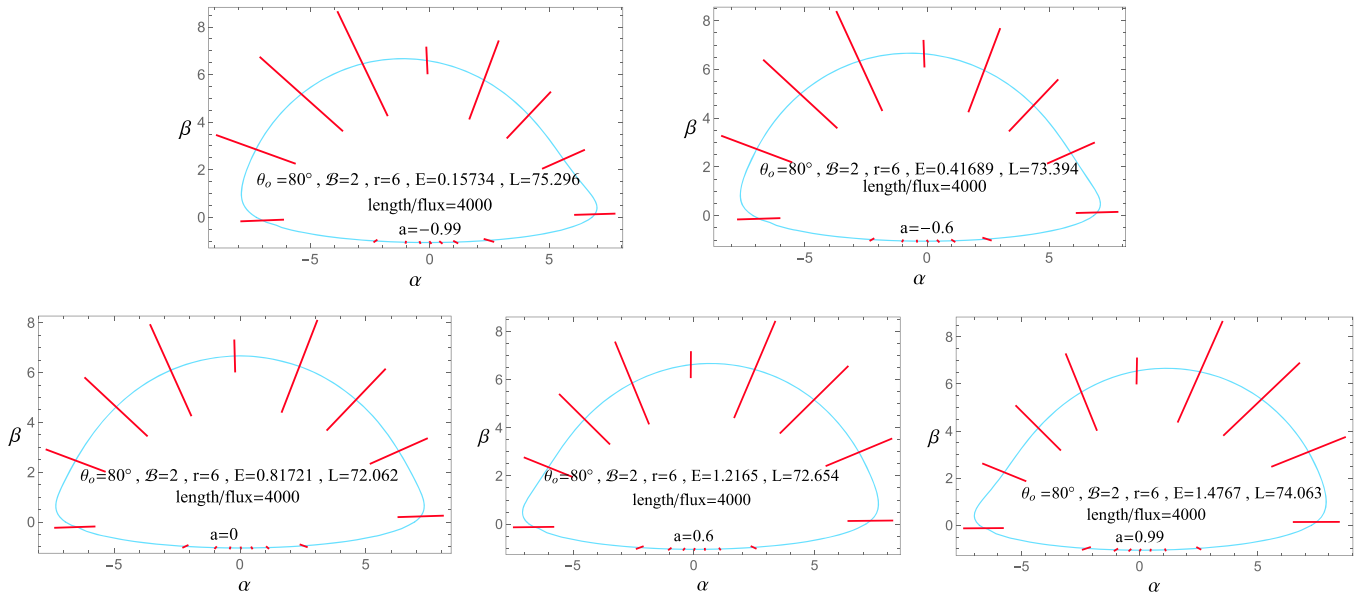FIG. 4.   Polarized images of charged particles in prograde orbits are produced with $\theta_o = 80°$, $\mathcal{B} = 2$, and $r_s = 6$. We let the spin a vary from -0.99 to 0.99. In this set of plots, we set length/flux = 4000.
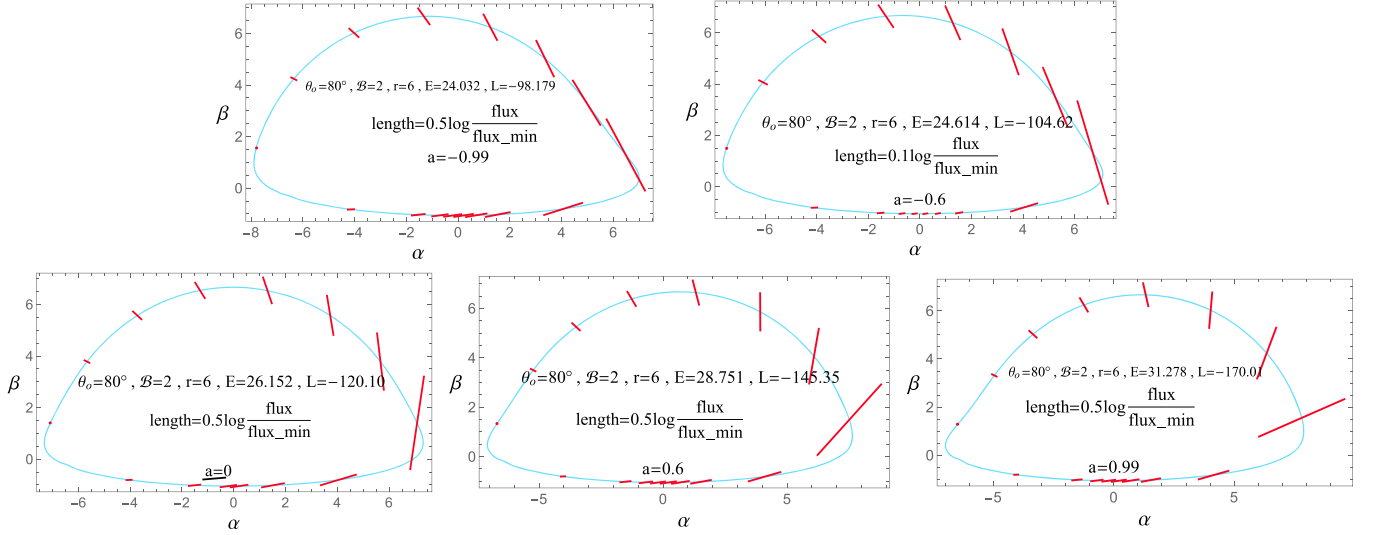
FIG. 5.   Polarized images of charged particles in retrograde orbits are produced with $\theta_o = 80°$, $r = 6$, and $\mathcal{B} = 2$. We also let the spin a vary from -0.99 to 0.99. The red line is scaled by taking the logarithm of flux for the sake of visualization, since the Doppler effect is powerful in this case.

$$(r_{\text{ISCO}})_{\text{SI}} = 1.5 \times 10^3 \, \frac{M}{M_\odot}. \qquad (3.15)$$

For a solar-mass black hole, the frequency of the particle would be

$$f \sim \frac{c}{2\pi r_{\text{ISCO}}} \simeq 30 \text{ kHz}, \qquad (3.16)$$

which may be at least technically observable. Nonetheless, for the supermassive black holes with a mass of $M \sim 10^9 M_\odot$, the frequency is roughly $f \sim 3 \times 10^{-5}$ Hz, which is conceivably unobservable for the ground-based telescope. Hence, it is more likely that the research in the present work can be applied only to the case of black holes of solar mass, from an observational perspective.[2]

IV. SUMMARY

In this work, we studied the circular motions and the polarized images of charged particles in the Kerr spacetime with a weak magnetic field. We focused on the case that the magnetic field and the charge-to-mass ratio are not large, which applies to many charged astrophysical clouds of dust and objects. In this case, the effective potential gets simplified and allows analytical treatment. We found an analytical expression of the radius of the ISCOs in terms of the energy density E and the angular momentum density L and obtained the constraints that E and L should satisfy. It is worth emphasizing that astrophysical objects widely exist in the Universe which help the condition $\mathcal{B} \ll 1$.

Thus, our simplified treatment and analytical results are helpful to relevant studies.

Moreover, we revisited how to calculate the polarized images, including the orbits of charged particles, polarization direction, and flux of the synchronize radiation following our previous work [36] to prepare for numerical computations. We obtained the images of circular orbits through the ray-tracing method. We presented several figures to show the polarized images of charged particles at fixed $\mathcal{B}$ and r_s, where r_s was the orbit radius of the source. We stress that, in studying the polarized images with the numerical method, we did not assume the approximate condition $\mathcal{B} \ll 1$, and our polarized photos were not limited to the case $\mathcal{B} \ll 1$.

From our study, we read the influences of the orbit directions, the spins of the black hole, and the observational angles on the polarized images. The images for the prograde and retrograde orbits are very different for the same orbit radius. For example, we found that the so-called Doppler beaming was evident for the retrograde orbits. In addition, we observed a significant influence of the spin a on the polarized images. More precisely, when a increases, the polarization angle rotates clockwise. This phenomenon becomes especially visible for retrograde orbits. The spin a also has a non-negligible effect on the magnitudes of polarization fluxes. Moreover, we showed the impacts of the observational angle on the polarized images.

It would be illuminating to compare our results with the ones in Ref. [33], which also studied the polarized images of equatorial emission in the Kerr geometry. In our study, we focused on a vertical magnetic field corresponding to $(B^r = 0, B^\phi = 0, B^{(\theta)})$ in Ref. [33]; somehow, however, our results were closer to the ones in their case $(B^r = 0,$

---

[2]We express our utmost gratitude to the anonymous reviewer for drawing our attention to this issue.

$B^{\phi}, B^{(\theta)} = 0$). The main reason is that the electromagnetic radiation in our model is purely from charged particles without self-interactions. At the same time, Ref. [33] assumed that the synchrotron radiation was from charged fluids, and, thus, the formulas of the polarization vector of the radiation are different. In addition, the configuration of the magnetic field is chosen in the frame of the source in Ref. [33], while we pick the configuration observed by the observers at infinity.

Moreover, the formula Eq. (3.1) for the polarization vector, which was directly derived from the Maxwell equation in curved spacetime, takes a covariant form and can easily be used in numerical studies. In contrast, the polarization vector in Ref. [33] is determined in a local frame.

[1] B. P. Abbott *et al.* (LIGO Scientific and Virgo Collaborations), Observation of Gravitational Waves from a Binary Black Hole Merger, Phys. Rev. Lett. **116,** 061102 (2016).

[2] B. P. Abbott *et al.* (LIGO Scientific and Virgo Collaborations), GW151226: Observation of Gravitational Waves from a 22-Solar-Mass Binary Black Hole Coalescence, Phys. Rev. Lett. **116,** 241103 (2016).

[3] B. P. Abbott *et al.* (LIGO Scientific and Virgo Collaborations), GW170817: Observation of Gravitational Waves from a Binary Neutron Star Inspiral, Phys. Rev. Lett. **119,** 161101 (2017).

[4] V. Lipunov, E. Gorbovskoy, V. Kornilov, N. Tyurina, P. Balanutsa, A. Kuznetsov, D. Vlasenko, D. Kuvshinov, I. Gorbunov, D. Buckley *et al.*, Master optical detection of the first LIGO/Virgo neutron star binary merger GW170817, Astrophys. J. Lett. **850,** L1 (2017).

[5] K. Akiyama *et al.* (Event Horizon Telescope Collaboration), First M87 Event Horizon Telescope Results. I. The shadow of the supermassive black hole, Astrophys. J. Lett. **875,** L1 (2019).

[6] K. Akiyama *et al.* (Event Horizon Telescope Collaboration), First M87 Event Horizon Telescope Results. III. Data processing and calibration, Astrophys. J. Lett. **875,** L3 (2019).

[7] K. Akiyama *et al.* (Event Horizon Telescope Collaboration), First M87 Event Horizon Telescope Results. IV. Imaging the central supermassive black hole, Astrophys. J. Lett. **875,** L4 (2019).

[8] K. Akiyama *et al.* (Event Horizon Telescope Collaboration), First M87 Event Horizon Telescope Results. V. Physical origin of the asymmetric ring, Astrophys. J. Lett. **875,** L5 (2019).

[9] K. Akiyama *et al.* (Event Horizon Telescope Collaboration), First M87 Event Horizon Telescope Results. VI. The shadow and mass of the central black hole, Astrophys. J. Lett. **875,** L6 (2019).

[10] K. Akiyama *et al.* (Event Horizon Telescope Collaboration), First Sagittarius A* Event Horizon Telescope Results. I. The shadow of the supermassive black hole in the center of the milky way, Astrophys. J. Lett. **930,** L12 (2022).

[11] R. D. Blandford and R. L. Znajek, Electromagnetic extractions of energy from Kerr black holes, Mon. Not. R. Astron. Soc. **179,** 433 (1977).

[12] R. M. Wald, Black hole in a uniform magnetic field, Phys. Rev. D **10,** 1680 (1974).

[13] M. Dovčiak, V. Karas, and G. Matt, Polarization signatures of strong gravity in active galactic nuclei accretion discs, Mon. Not. R. Astron. Soc. **355,** 1005 (2004).

[14] M. Zajaček, A. Tursunov, A. Eckart, S. Britzen, E. Hackmann, V. Karas, Z. Stuchlík, B. Czerny, and J. A. Zensus, Constraining the charge of the Galactic centre black hole, J. Phys. Conf. Ser. **1258,** 012031 (2019).

[15] R. A. Daly, Black hole spin and accretion disk magnetic field strength estimates for more than 750 active galactic nuclei and multiple galactic black holes, Astrophys. J. **886,** 37 (2019).

[16] M. Y. Piotrovich, N. A. Silant'ev, Y. N. Gnedin, and T. M. Natsvlishvili, Magnetic fields of black holes and the variability plane, arXiv:1002.4948.

[17] K. Akiyama *et al.* (Event Horizon Telescope Collaboration), First M87 Event Horizon Telescope Results. VII. Polarization of the ring, Astrophys. J. Lett. **910,** L12 (2021).

[18] K. Akiyama *et al.* (Event Horizon Telescope Collaboration), First M87 Event Horizon Telescope Results. VIII. Magnetic field structure near The Event Horizon, Astrophys. J. Lett. **910,** L13 (2021).

[19] R. Narayan, D. C. Palumbo, M. D. Johnson, Z. Gelles, E. Himwich, D. O. Chang, A. Ricarte, J. Dexter, C. F. Gammie, A. A. Chael *et al.*, The polarized image of a synchrotron-emitting ring of gas orbiting a black hole, Astrophys. J. **912,** 35 (2021).

[20] E. Himwich, M. D. Johnson, A. Lupsasca, and A. Strominger, Universal polarimetric signatures of the black hole photon ring, Phys. Rev. D **101,** 084020 (2020).

[21] V. P. Frolov and A. A. Shoom, Motion of charged particles near a weakly magnetized schwarzschild black hole, Phys. Rev. D **82,** 084034 (2010).

[22] A. M. A. Zahrani, Charged particle circular orbits around weakly charged and magnetized Kerr black holes, Astrophys. J. **937**, 50 (2022).

[23] R. Shiose, M. Kimura, and T. Chiba, Motion of charged particles around a weakly magnetized rotating black hole, Phys. Rev. D **90**, 124016 (2014).

[24] A. M. Al Zahrani, Escape of charged particles moving around a weakly magnetized Kerr black hole, Phys. Rev. D **90**, 044012 (2014).

[25] F. J. Ernst, Black holes in a magnetic universe, J. Math. Phys. (N.Y.) **17**, 54 (1976).

[26] E. F. J. and W. W. J., Kerr black holes in a magnetic universe, J. Math. Phys. (N.Y.) **17**, 182 (1976).

[27] Y.-K. Lim, Motion of charged particles around a magnetized/electrified black hole, Phys. Rev. D **91**, 024048 (2015).

[28] H. Zhu and M. Guo, Polarized image of synchrotron radiations of hotspots in Schwarzschilld-Melvin black hole spacetime, arXiv:2205.04777.

[29] D. Li and X. Wu, Chaotic motion of neutral and charged particles in a magnetized Ernst-Schwarzschild spacetime, Eur. Phys. J. Plus **134**, 96 (2019).

[30] A. Ricarte, R. Qiu, and R. Narayan, Black hole magnetic fields and their imprint on circular polarization images, Mon. Not. R. Astron. Soc. **505**, 523 (2021).

[31] A. Lupsasca, D. Kapec, Y. Shi, D. E. A. Gates, and A. Strominger, Polarization whorls from M87* at the Event Horizon Telescope, Proc. R. Soc. A **476**, 20190618 (2020).

[32] K. Akiyama *et al.* (Event Horizon Telescope Collaboration), The polarized image of a synchrotron-emitting ring of gas orbiting a black hole, Astrophys. J. **912**, 35 (2021).

[33] Z. Gelles, E. Himwich, D. C. M. Palumbo, and M. D. Johnson, Polarized image of equatorial emission in the Kerr geometry, Phys. Rev. D **104**, 044060 (2021).

[34] X. Qin, S. Chen, and J. Jing, Polarized image of an equatorial emitting ring around a 4D Gauss–Bonnet black hole, Eur. Phys. J. C **82**, 784 (2022).

[35] Z. Zhang, S. Chen, X. Qin, and J. Jing, Polarized image of a Schwarzschild black hole with a thin accretion disk as photon couples to Weyl tensor, Eur. Phys. J. C **81**, 991 (2021).

[36] Z. Hu, Y. Hou, H. Yan, M. Guo, and B. Chen, Polarized images of synchrotron radiations in curved spacetime, Eur. Phys. J. C **82**, 1166 (2022).

[37] X. Qin, S. Chen, Z. Zhang, and J. Jing, Polarized image of a rotating black hole in Scalar–Tensor–Vector–Gravity theory, Astrophys. J. **938**, 2 (2022).

[38] T. C. Quinn and R. M. Wald, An axiomatic approach to electromagnetic and gravitational radiation reaction of particles in curved space-time, Phys. Rev. D **56**, 3381 (1997).

[39] A. Al Zahrani, Charged particle circular orbits around weakly charged and magnetized Kerr black holes, Astrophys. J. **937**, 50 (2022).

[40] Y. Hou, P. Liu, M. Guo, H. Yan, and B. Chen, Multi-level images around Kerr–Newman black holes, Classical Quantum Gravity **39**, 194001 (2022).

[41] M. Guo, N. A. Obers, and H. Yan, Observational signatures of near-extremal Kerr-like black holes in a modified gravity theory at the Event Horizon Telescope, Phys. Rev. D **98**, 084063 (2018).